Molecular Cancer Therapeutics

Efficacy of PARP Inhibitor Rucaparib in Orthotopic Glioblastoma Xenografts Is Limited by Ineffective Drug Penetration into the Central Nervous System

Karen E. Parrish[1], Ling Cen[2], James Murray[3], David Calligaris[4], Sani Kizilbash[5], Rajendar K. Mittapalli[1], Brett L. Carlson[2], Mark A. Schroeder[2], Julieann Sludden[3], Alan V. Boddy[3], Nathalie Y.R. Agar[4,6,7], Nicola J. Curtin[3], William F. Elmquist[1], and Jann N. Sarkaria[1]

Abstract

PARP inhibition can enhance the efficacy of temozolomide and prolong survival in orthotopic glioblastoma (GBM) xenografts. The aim of this study was to evaluate the combination of the PARP inhibitor rucaparib with temozolomide and to correlate pharmacokinetic and pharmacodynamic studies with efficacy in patient-derived GBM xenograft models. The combination of rucaparib with temozolomide was highly effective *in vitro* in short-term explant cultures derived from GBM12, and, similarly, the combination of rucaparib and temozolomide (dosed for 5 days every 28 days for 3 cycles) significantly prolonged the time to tumor regrowth by 40% in heterotopic xenografts. In contrast, the addition of rucaparib had no impact on the efficacy of temozolomide in GBM12 or GBM39 orthotopic models. Using Madin-Darby canine kidney (MDCK) II cells stably expressing murine BCRP1 or human MDR1, cell accumulation studies demonstrated that rucaparib is transported by both transporters. Consistent with the influence of these efflux pumps on central nervous system drug distribution, *Mdr1a/b*$^{-/-}$*Bcrp1*$^{-/-}$ knockout mice had a significantly higher brain to plasma ratio for rucaparib (1.61 ± 0.25) than wild-type mice (0.11 ± 0.08). A pharmacokinetic and pharmacodynamic evaluation after a single dose confirmed limited accumulation of rucaparib in the brain is associated with substantial residual PARP enzymatic activity. Similarly, matrix-assisted laser desorption/ionization mass spectrometric imaging demonstrated significantly enhanced accumulation of drug in flank tumor compared with normal brain or orthotopic tumors. Collectively, these results suggest that limited drug delivery into brain tumors may significantly limit the efficacy of rucaparib combined with temozolomide in GBM. *Mol Cancer Ther; 14(12); 2735–43. ©2015 AACR.*

Introduction

Temozolomide chemotherapy combined with radiation followed by temozolomide alone can significantly extend survival for a subset of patients with glioblastoma multiforme (GBM). Unfortunately, essentially all patients recur following therapy, and the median survival for patients with GBM is slightly longer than 1 year (1, 2). One novel therapeutic strategy being explored to extend the survival for these patients is inhibition of DNA repair by PARP inhibitors during chemotherapy. PARP1 and 2 are nuclear enzymes that play key roles in the modulation of DNA repair. In response to a variety of DNA damages, PARP binds to sites of DNA damage, catalyzes the poly(ADP-ribosyl)ation of target proteins and recruits DNA repair proteins to these sites. Consistent with the importance of PARP in DNA repair, inhibition of PARP activity in combination with temozolomide or other chemotherapy agents can markedly enhance the efficacy of therapy (3–7). These studies have driven significant interest in developing PARP inhibitors for clinical use in combination with cytotoxic chemotherapies.

At least eight small-molecule inhibitors targeting PARP have been developed as clinical drugs by major pharmaceutical companies and are being tested for cancer indications in clinical trials (8). The first PARP inhibitor to be evaluated in clinical trials was rucaparib (AG014699). Multiple preclinical studies have demonstrated that rucaparib can markedly enhance the efficacy of temozolomide in a variety of solid tumor models (9–11). In a phase I clinical trial, rucaparib was well tolerated in combination with temozolomide in patients with advanced melanoma, and a pharmacodynamic analysis demonstrated robust suppression of PARP activity in peripheral tumors at clinically achievable doses (12). In a subsequent phase II study of patients with metastatic melanoma treated with both rucaparib and temozolomide, the combination was safe and was associated with an improvement in

[1]Department of Pharmaceutics, University of Minnesota, Minneapolis, Minnesota. [2]Department of Radiation Oncology, Mayo Clinic, Rochester, Minnesota. [3]Newcastle University, Newcastle upon Tyne, United Kingdom. [4]Department of Neurosurgery, Brigham and Women's Hospital, Harvard Medical School, Boston, Massachusetts. [5]Department of Medical Oncology Mayo Clinic, Rochester, Minnesota. [6]Department of Radiology, Brigham and Women's Hospital, Harvard Medical School, Boston, Massachusetts. [7]Department of Cancer Biology, Dana-Farber Cancer Institute, Harvard Medical School, Boston, Massachusetts.

Note: Supplementary data for this article are available at Molecular Cancer Therapeutics Online (http://mct.aacrjournals.org/).

K.E. Parrish and L. Cen contributed equally to this article.

Corresponding Author: Jann N. Sarkaria, Mayo Clinic, 200 First St. SW, Rochester, MN 55905. Phone: 507-284-8227; Fax: 507-284-0079; E-mail: sarkaria.jann@mayo.edu

doi: 10.1158/1535-7163.MCT-15-0553

progression-free survival when compared with historical controls (13). Clinical trials in patients with metastatic breast and advanced ovarian cancer are currently evaluating rucaparib, both as a single agent and in combination with platinum-based chemotherapy (14–19). In anticipation of developing a clinical trial for patients with GBM, we performed a preclinical evaluation of rucaparib in combination with temozolomide in GBM xenograft models. Our results demonstrate that rucaparib is excluded from the central nervous system (CNS) by the blood–brain barrier (BBB) and has limited efficacy in an orthotopic GBM xenograft model.

Materials and Methods

In vitro neurosphere formation assay

Short-term explant cultures of GBM12 were seeded in triplicate in a 96-well plate in neural stem cell serum-free media (A10509-01, Life Technologies). Temozolomide with or without rucaparib were added 24 hours later. The number of neurospheres formed was counted in each well after 14 days (20).

In vitro accumulation

In vitro intracellular accumulation experiments were conducted in vector controlled Madin-Darby canine kidney II (MDCKII) cells or MDCKII cells that overexpress either human multidrug resistance protein 1 (MDR1) or murine Breast Cancer Resistance Protein (BCRP1) as previously described (21). Bcrp1-transfected cells were a gift from Dr. Alfred Schinkel *circa* 2003 (The Netherlands Cancer Institute) and MDR1-transfected cells were provided by Dr. Piet Borst in *circa* 1996 (The Netherlands Cancer Institute). Studies using radiolabeled prazosin and vinblastine were used as positive controls for Bcrp and MDR1 function to authenticate transporter activity. Cells were seeded at a density of 2×10^5 cells per well in 24-well polystyrene plates (Corning Glassworks) and grown to 80% confluence. Cells were washed with serum-free assay buffer, and then preincubated for 30 minutes in either buffer alone or buffer with a specific inhibitor for MDR1 (1 μmol/L LY335979) or BCRP1 (0.2 μmol/L KO143). Cells were incubated with 2 μmol/L rucaparib for 60 minutes at 37°C and then transport was quenched with cold PBS prior to lysis in 1% Triton X-100. Cell pellets were stored at −80°C until analysis using high-performance liquid chromatography followed by tandem mass spectrometry (LC/MS-MS). The intracellular concentrations of rucaparib were normalized to the protein concentration determined by a BCA protein assay.

GBM xenograft model and therapy response evaluation

All animal experiments were reviewed and approved by the Mayo Clinic or University of Minnesota Institutional Animal Care and Use Committee. Drug efficacy was evaluated using GBM patient–derived xenografts from the Mayo panel using either orthotopic or flank glioblastoma xenograft models (22). All patient-derived xenograft cell lines were obtained from patients at the Mayo Clinic and maintained exclusively by serial passage in mice. Mice with established intracranial xenografts for GBM12, GBM14, GBM39, GBM43, and GBM59 were randomized into treatment groups of 10 mice each and treated with either placebo, rucaparib (1 mg/kg days 1–5 every 28 days × 3 cycles), temozolomide (50 mg/kg days 1–5 every 28 days × 3 cycles), or temozolomide concurrent with rucaparib. Rucaparib was a gift from Pfizer, dissolved in dimethylsulfoxide and diluted in saline for intraperitoneal injection. Temozolomide was purchased from the Mayo Clinic Pharmacy, suspended in Ora-plus (Paddock Laboratories), and administered by oral gavage. All intracranial tumor-bearing animals used for therapy evaluation were observed daily and euthanized once they reached a moribund condition. Treatment of flank tumor xenografts was essentially the same with the exception that tumor volume was measured three times weekly. The endpoint for the flank study was time for tumors to exceed 1,000 mm^3. To evaluate BBB integrity in orthotopic tumors, mice were injected with TexasRed-3 kDa dextran conjugate, euthanized by saline perfusion 10 minutes later, and then processed as described previously (23).

Steady-state assessment of rucaparib in brain

The steady state brain distribution of rucaparib was evaluated in wild-type, and *Mdr1a/b*$^{-/-}$*Bcrp1*$^{-/-}$ mice. Rucaparib (5 mg/mL in DMSO) was administered at a rate of 5 μg/hour using rucaparib-loaded osmotic mini pumps (Durect Corporation) as described previously (24). Animals were euthanized 48 hours after pump implantation, and plasma and brain were flash frozen and stored at −80°C until analysis by LC/MS-MS.

Analysis of rucaparib samples by LC/MS-MS Assay

Brain samples were homogenized in 5% bovine serum albumin and samples (cell lysate, plasma, or brain homogenate) were spiked with an internal standard (dasatinib). After extraction in ice-cold ethyl acetate, the organic supernatant was dried under nitrogen, reconstituted in the mobile phase (70:30 of 20 mmol/L ammonium formate with 0.1% formic acid: acetonitrile), and injected onto the column (Phenomenex Synergi Polar 4 μ polar-RP 80A column; 75 × 2 mm). The ionization was conducted in positive mode and the m/z transitions were 292 and 401 for rucaparib and dasatinib, respectively.

Evaluation of rucaparib pharmacokinetics and PARP activity in xenografts

An initial evaluation of rucaparib pharmacokinetics was performed in mice with orthotopic GBM12 xenografts treated with a single 1 mg/kg dose of rucaparib. Plasma, liver, and brain were harvested and flash frozen at 0, 60, 120, 360, and 1,440 minutes after injection. Rucaparib levels were measured by LC/MS as described previously (11, 12). The same tissue samples were processed in a PARP enzymatic assay (9, 11, 12). Briefly, tumor, brain, and liver homogenates were diluted (1:9,000, 1:2,000, and 1:3,000, respectively) and incubated with a double-stranded oligonucleotide and excess NAD^+. The formation of ADP-ribose polymer was quantified by immunoblotting with the antiPAR 10H Ab (kind gift from Alex Burkle, University of Konstanz) and normalized to protein levels (BCA assay) in the homogenate.

Matrix-assisted laser desorption/ionization mass spectrometric imaging analysis

Mice with established tumors received a single dose of rucaparib (10 mg/kg) intraperitoneally and brain, liver, and tumor were snap frozen in liquid nitrogen. Twelve micron cryosections were thaw mounted onto ITO-coated microscopic slides (Bruker Daltonics) for MALDI MSI and onto optical slides for hematoxylin and eosin staining. After sample drying in a desiccator, a 2,5-dihydroxybenzoic acid matrix (DHB, 160 mg/mL solution in methanol/0.2% TFA 70:30 v/v) was deposited using a TM sprayer (HTX imaging) with the following conditions: flow rate,

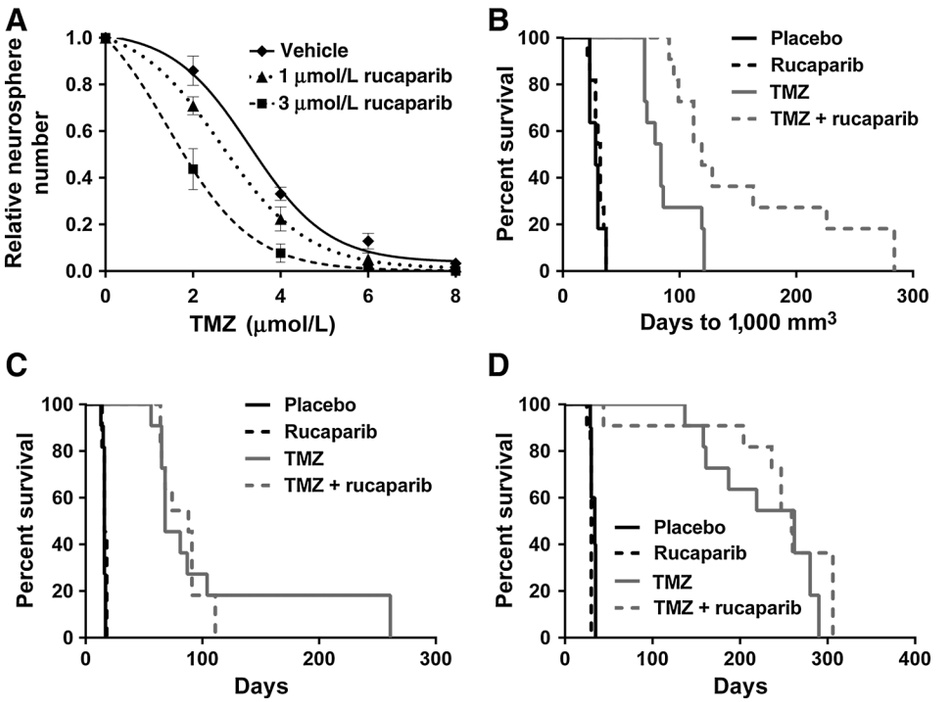

Figure 1.
Efficacy of rucaparib combined with temozolomide in GBM xenograft models. A, effects of rucaparib in combination of temozolomide were evaluated using short-term explant culture obtained from GBM12 xenograft tumor in a neurosphere formation assay. B, mice with GBM12 flank xenografts were randomized and treated with placebo, rucaparib 1 mg/kg/day, days 1–5 every 28 days × 3 cycles, temozolomide 50 mg/kg/day, days 1–5 every 28 days × 3 cycles, or the combination. Time for tumors to exceed 1,000 mm^3 in volume is shown. Survival curve for mice with established orthotopic GBM12 (C) or GBM39 (D) xenografts were randomized and treated as above. Animals were followed until reaching a moribund state. Differences between treatment groups were compared using log-rank test.

90 μL/minute; spray nozzle velocity, 1,200 mm/minute; spray nozzle temperature, 75°C; nitrogen gas pressure, 10 psi; track spacing, 2 mm; number of passes, 4.

Mass spectra were acquired using a 12 Tesla SolariX XR Fourier transform ion cyclotron resonance mass spectrometer (FT-ICR MS) (Bruker Daltonics), externally calibrated in electrospray ionization positive ion mode using arginine clusters. MALDI MS images were acquired with a pixel step size for the surface raster set to 80 μm for brain and liver sections, and to 100 μm for flank tumor sections. Spectra were acquired in positive ion mode from 250 laser shots accumulated at each spot with a mass range of m/z 100 to 2,500. The laser intensity was set to 40% with a frequency of 1,000 Hz. MALDI images were displayed and analyzed using the software FlexImaging 4.0. Images were displayed following the signal of rucaparib (m/z 324.1507 ± 0.001, Supplementary Fig. S1) and heme as a biomarker of the vasculature (m/z 616.1768 ± 0.001) as previously described (25).

Statistical analysis

The data are presented as mean ± standard deviation of the mean. A two-sample t test was used to compare continuous measures across groups. Survival distributions were estimated using the Kaplan–Meier method. The log-rank test was used to compare survival across groups. The criteria for statistical significance were taken as two-tailed P values < 0.05.

Results

Efficacy of rucaparib *in vitro* and *in vivo*

The combination of rucaparib and temozolomide was evaluated initially in the Mayo GBM12 primary GBM xenograft line. This MGMT hypermethylated xenograft line is sensitive to temozolomide and is highly responsive to the temozolomide-sensitizing effects of the PARP inhibitor veliparib (26). In a neurosphere formation assay, rucaparib significantly enhanced the efficacy of temozolomide in GBM12 cells *in vitro*. The unbound concentration required to inhibit 50% (IC_{50}) neurosphere formation was 3.3 ± 0.4 μmol/L for monotherapy with temozolomide while the IC_{50} was reduced to 2.7 ± 0.3 and 1.9 ± 0.3 μmol/L temozolomide when used in combination with 1 and 3 μmol/L rucaparib, respectively (Fig. 1A; $P = 0.0148$ and $P < 0.0001$). Using these same GBM12 cells, flank xenografts were established and mice were randomized to therapy with placebo or temozolomide (50 mg/kg days 1–5) with or without rucaparib (1 mg/kg days 1–5) given over three 28 day cycles. Rucaparib significantly potentiated temozolomide-induced tumor regrowth delay in a flank tumor model of GBM12. Median time for tumor to exceed a 1,000 mm^3 size endpoint for placebo, temozolomide, and temozolomide/rucaparib treatment was 32, 86, and 121 days, $P < 0.01$, respectively (Fig. 1B). In contrast, the addition of rucaparib to temozolomide therapy in GBM12 orthotopic xenografts was ineffective (median survival: placebo 16 days, temozolomide 68 days and temozolomide/rucaparib 81 days, $P = 0.88$, Fig. 1C). A similar lack of efficacy was observed in four other primary GBM xenograft models, including GBM39 (Fig. 1D and Supplementary Fig. S2). The combination of temozolomide and the PARP inhibitor veliparib is highly effective in orthotopic models for both GBM12 and GBM39 (26, 27), and a similar sensitizing effect for veliparib/temozolomide combination is observed in heterotopic model for GBM12 (27). Therefore, subsequent studies focused on evaluating whether exclusion of rucaparib from the brain and orthotopic brain tumors might contribute to the lack of efficacy observed in the orthotopic xenograft models.

Intracellular accumulation of rucaparib

The ATP-binding cassette (ABC) transporters multidrug resistance 1 (MDR1) and breast cancer resistance protein (BCRP1)

are located in the luminal membrane of brain capillary endothelial cells and function within the BBB to limit drug accumulation in the brain (28–30). The intracellular accumulation of rucaparib was evaluated in MDCKII vector controlled (WT) and MDR1- or BCRP1-overexpressing cell lines to determine whether rucaparib was a substrate for these efflux pumps. The intracellular accumulation of rucaparib in MDCKII WT and MDR1 or BCRP1 overexpressing cell lines was compared with prototypical substrates for these two efflux pumps to determine the efflux liability of rucaparib. Intracellular drug accumulation was significantly reduced in MDR1-expressing cells in comparison with vector controlled cells, for both vinblastine (20.1 ± 2.6% of control, $P < 0.05$) and rucaparib (32.0 ± 7.4% of control, $P < 0.05$, Fig. 2A). Cotreatment with a specific MDR1 inhibitor LY335979 abolished the diminished uptake of either vinblastine or rucaparib in the MDR1 overexpressing line. Similarly, BCRP1 overexpression resulted in a marked suppression of intracellular accumulation of prazosin (16.8 ± 1.4% of control, $P < 0.05$) and rucaparib (14.5 ± 5.2% of control, $P < 0.05$), and cotreatment with the specific BCRP1 inhibitor Ko143 eliminated any differential uptake between the vector controlled and BCRP1 overexpressing lines (Fig. 2B). These data show that rucaparib is a substrate for both MDR1 and BCRP1 efflux pumps.

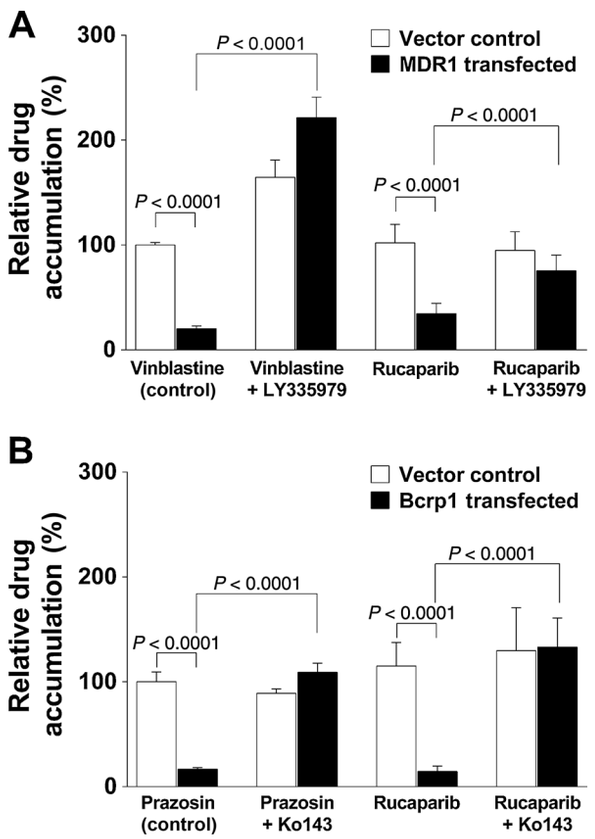

Figure 2.
Intracellular accumulation of rucaparib in MDCKII cells. A, vector control and MDR1-overexpressing MDCKII cells were treated with vinblastine (9.3 nmol/L) or rucaparib (2 μmol/L) in the presence or absence of the MDR1 inhibitor LY335979 and intracellular levels of vinblastine or rucaparib were measured. B, wild-type and BCRP1-overexpressing MDCKII cells were treated with prazosin (0.39 nmol/L) or rucaparib (2 μmol/L) in the presence or absence of the BCRP1 inhibitor Ko143 and intracellular levels of prazosin or rucaparib were measured. Results are presented as mean ± SD; $n = 5$–6.

Brain distribution in FVB wild-type and Mdr1a/1b$^{-/-}$;Bcrp1$^{-/-}$ mice

Steady-state concentrations in brain and plasma were determined in wild-type (WT) and in triple knockout (TKO: *Mdr1a/1b*$^{-/-}$;*Bcrp1*$^{-/-}$) mice. The TKO mice lack expression of MDR1 and BCRP1 proteins and comparison with wild-type mice will show the influence of these efflux transporters on rucaparib brain delivery. After a 48-hour continuous intraperitoneal infusion via osmotic pump, brain and plasma concentrations of rucaparib were determined in both WT and TKO mice (Fig. 3A). Brain accumulation of rucaparib was significantly increased in the TKO mice (brain to plasma ratio of 1.61 ± 0.25) as compared with wild-type mice (brain to plasma ratio of 0.11 ± 0.08; $P = 0.0001$, see Fig. 3B). In conjunction with the *in vitro* data, these *in vivo* data clearly show that MDR1 and BCRP1 activity at the BBB significantly limits the accumulation of rucaparib within the CNS.

Pharmacokinetic and pharmacodynamic analysis of rucaparib

The accumulation of rucaparib and effects on PARP inhibition were evaluated in mice with established orthotopic xenografts. Plasma and tissue distribution was quantified over the course of 24 hours after a single intraperitoneal injection of drug (Fig. 4A and B). The concentration of rucaparib in plasma was highest at the first 60-minute time point (0.34 μmol/L) and exhibited a half-life of 1.5 hours. Distribution of rucaparib at 60 minutes was similar in the tumor-injected hemisphere (0.35 μmol/L), significantly higher in liver (11.05 μmol/L), and markedly lower in the contralateral brain hemisphere (0.08 μmol/L). Interestingly, in the tumor-injected hemisphere, rucaparib showed a significant retention even at 6 hours (0.23 μmol/L) and an apparent half-life of 13.0 hours. Albeit at much lower levels, rucaparib also accumulated in normal brain, but levels were undetectable by 360 minutes after injection. Thus, in comparison with liver tissue levels, rucaparib had significantly lower accumulation in normal brain and intermediate accumulation in tumor-bearing brain.

Rucaparib causes prolonged suppression of PARP activity, even after short exposure (31), and because of this, the inhibitory effects of rucaparib on PARP activity in tissues can be measured directly in a PARP enzyme activity assay. Using the same tissue samples processed for drug level determination, the extent of PARP activity suppression was evaluated and reported here as the pmol of PAR formation per μg of protein (Fig. 4C). Baseline PARP activity was highest in the tumor-injected hemisphere (41.4 pmol/μg protein) in comparison with the contralateral hemisphere (11.8 pmol/μg protein) or liver (7.4 pmol/μg protein). The extent of PARP activity suppression was greatest in liver, in which PARP activity was reduced to 5% of baseline for several hours and recovered to 68% of baseline by 24 hours (Fig. 4D). Tissues recovered included liver and both hemispheres of the brain: the hemisphere contralateral to tumor injection is largely free of tumor and the tumor-injected hemisphere is significantly replaced by tumor (see Fig. 5). The entire tumor-bearing hemisphere was used in this analysis due to the highly infiltrative and semisolid properties of GBM12, which preclude reliable dissection of tumor from the

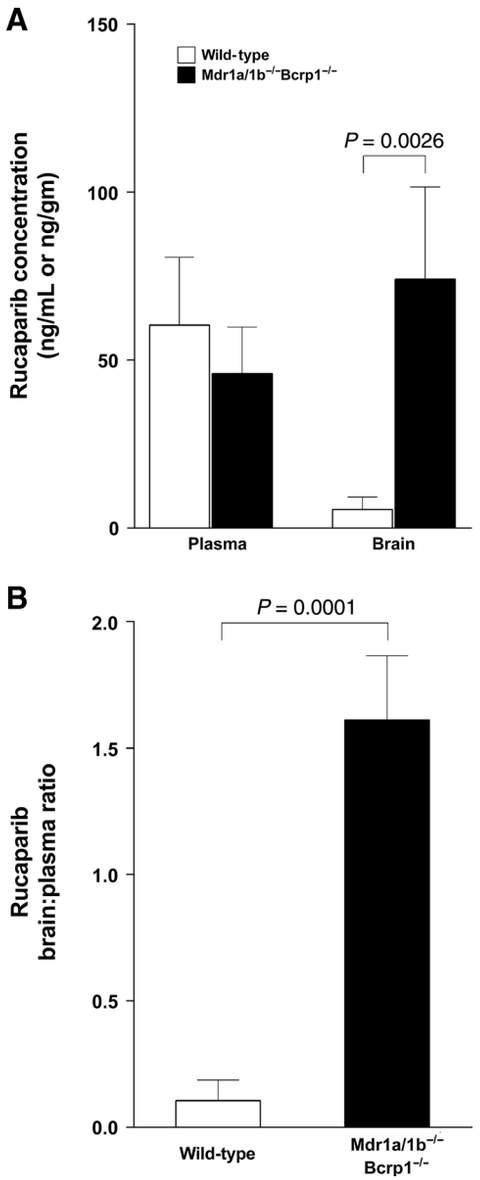

Figure 3.
Steady-state brain distribution of rucaparib in FVB wild-type (WT) and *Mdr1a/1b*$^{-/-}$*Bcrp1*$^{-/-}$ triple knock-out (TKO) mice. A, steady-state brain and plasma concentrations following a 48 hour intraperitoneal infusion at 5 μg/hour. B, rucaparib brain-to-plasma ratio at steady state. Following the 48 hour intraperitoneal infusion using an osmotic pump to deliver rucaparib at 5 μg/hour, blood and whole-brain were collected and analyzed for rucaparib concentration by LC/MS-MS. Values are presented as mean ± SD; $n = 4$.

surrounding brain tissue. PARP activity in the normal brain was reduced only to 62% of baseline at 60 minutes and recovered to baseline by 360 minutes after injection. In contrast, the tumor-injected hemisphere PARP activity was reduced to 50% of baseline but remained suppressed at this level for 24 hours. Thus, while PARP inhibition was more profound in liver, inhibition of PARP activity in the tumor-injected hemisphere was sustained for a longer duration.

BBB integrity in GBM12 orthotopic xenograft

Maintenance of tight junctions between brain capillary endothelial cells is critical for the preservation of a BBB, and the integrity of these tight junctions often is disrupted in GBM. Therefore, the integrity of the BBB was assessed in orthotopic GBM12 xenografts using Texas Red-3 kDa dextran conjugate, which accumulates in brain only in regions of tight junction disruption. Ten minutes after Texas Red–dextran administration, mice were euthanized and brains were removed for sectioning and analysis by confocal microscopy. As seen in Fig. 5, the distribution of Texas Red–dextran within the tumor was heterogeneous, with significant portions of the tumor demonstrating robust Texas Red–dextran accumulation, while other tumor regions had little to no accumulation. These data demonstrate that subregions of GBM12 orthotopic tumors have a relatively intact BBB.

Distribution of rucaparib in flank and orthotopic tumors

The distribution of rucaparib in flank and orthotopic GBM12 tumors was evaluated using two-dimensional MALDI-MSI (Fig. 6). Thirty minutes after a single intraperitoneal dose, homogeneous and high-level accumulation of rucaparib was observed in flank tumors (Fig. 6A, $n = 2$). In contrast, no appreciable rucaparib signal was observed either in orthotopic tumors ($n = 3$) or adjacent normal brain (Fig. 6B), while biomolecules associated with tumor or normal brain could be readily detected (Fig. 6i–iii). These data demonstrate that accumulation of rucaparib into both normal brain and orthotopic GBM12 tumors was below the level of detection for the MALDI-MSI technique compared with robust detection of drug in flank tumors.

Discussion

The combination of PARP inhibitors and temozolomide has been investigated in many cancers including glioblastoma multiforme (3–7, 26). We previously demonstrated robust chemosensitizing effects of the PARP inhibitor veliparib in primary GBM orthotopic and flank tumor xenograft models, including the MGMT methylated GBM12 and GBM39 primary xenograft orthotopic models (26, 27). Consistent with previous *in vivo* studies in colorectal cancer, neuroblastoma and medulloblastoma, rucaparib substantially potentiated temozolomide in flank tumor models of GBM12 (9–11). However, rucaparib did not potentiate temozolomide in orthotopic GBM models of GBM12, GBM 39, or three other primary GBM xenograft lines. The stark contrast in efficacy of the combination in the GBM12 flank versus orthotopic models and the biochemical data demonstrating liability for exclusion from brain distribution by BBB efflux pumps suggests that limited distribution of rucaparib into brain tumors may account for the lack of efficacy of rucaparib in the orthotopic models.

GBM tumors are characterized by heterogeneous disruption of the BBB. Under normal conditions, radiographic contrast material is physically excluded from the brain by tight junctions between brain capillary endothelial cells that form a physical BBB. Tumor-induced cytokines such as VEGF (alternatively known as vascular permeability factor) lead to disruption of tight junctions in regions of tumor that allow contrast material to accumulate in essentially all GBM (32). However, the extent

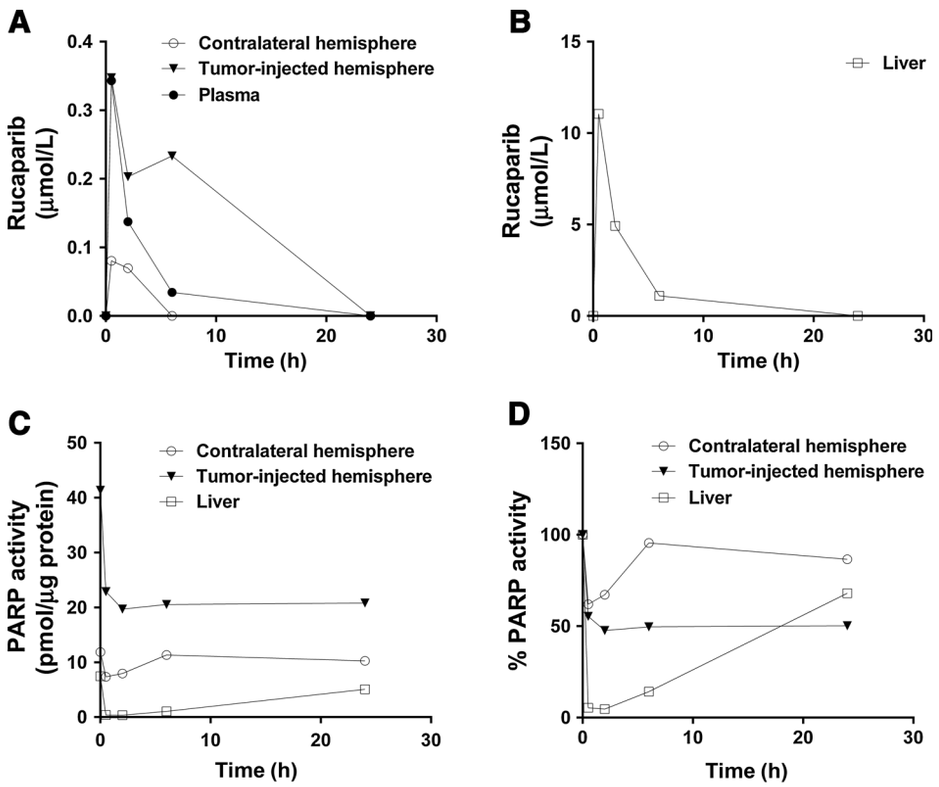

Figure 4.
Rucaparib concentration-time data and PARP inhibition in GBM12 orthotopic xenografts. Following a single dose of rucaparib (1 mg/kg), samples and tissues were collected at the indicated times. A, concentrations of rucaparib in plasma, tumor-injected and contralateral hemisphere of mouse brain, and liver (B) from orthotopic GBM12 xenograft mice. Concentrations of rucaparib at each time point are the mean from 2 or 3 tumor-bearing mice. Absolute (C) and relative PARP activity (D) in the same tissue samples were measured and plotted.

of contrast accumulation within an individual tumor can be highly heterogeneous, and neurosurgical studies have demonstrated that significant tumor burden is present in adjacent regions of tumor outside the contrast enhancing portion of GBM (33–35). Moreover, beyond any radiographic abnormality, isolated tumor cells infiltrate into normal brain tissue where the BBB is intact (23, 36). Similar to radiographic contrast, Texas Red 3 kDa–dextran can only accumulate in brain tumor regions with a disrupted BBB (23, 37). As in the clinical scenario, the Texas Red signal in GBM12 intracranial tumors is highly heterogeneous with lack of red fluorescence in significant portions of the tumor. Similar results have been observed in other orthotopic xenograft and genetically engineered models of glioma (23). Collectively, these data demonstrate that GBM12, and likely the other orthotopic xenograft models studied have at least some regions of tumor residing behind an intact BBB.

Drug efflux pumps expressed on the luminal surface of endothelial cells provide a biochemical BBB that complements the physical BBB provided by tight junctions between endothelial cells. MDR1 and BCRP1 are ATP-binding cassette (ABC) transporters in brain capillary endothelial cells that limit brain penetration of lipophilic drugs by actively transporting substrate molecules back into the bloodstream (38, 39). Using the canine kidney distal tubule–derived MDCKII epithelial cell line overexpressing either MDR1 or BCRP1, exclusion of rucaparib from the respective cells and reversal of this effect by specific efflux pump inhibitors demonstrates that rucaparib is an efflux substrate for both pumps. Consistent with the importance of these efflux pumps for exclusion of rucaparib from the

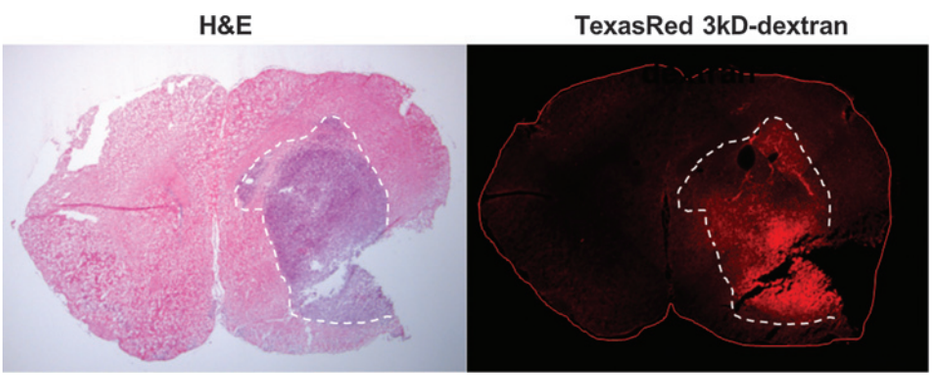

Figure 5.
Evaluation of blood-brain barrier integrity in GBM12. Mice with established GBM12 orthotopic xenografts were injected with Texas Red-3 kDa dextran conjugate and euthanized 10 minutes later. Shown are representative hematoxylin/eosin (H&E)-stained bright-field photomicrograph and a corresponding fluorescence photomicrograph of a serial unstained section.

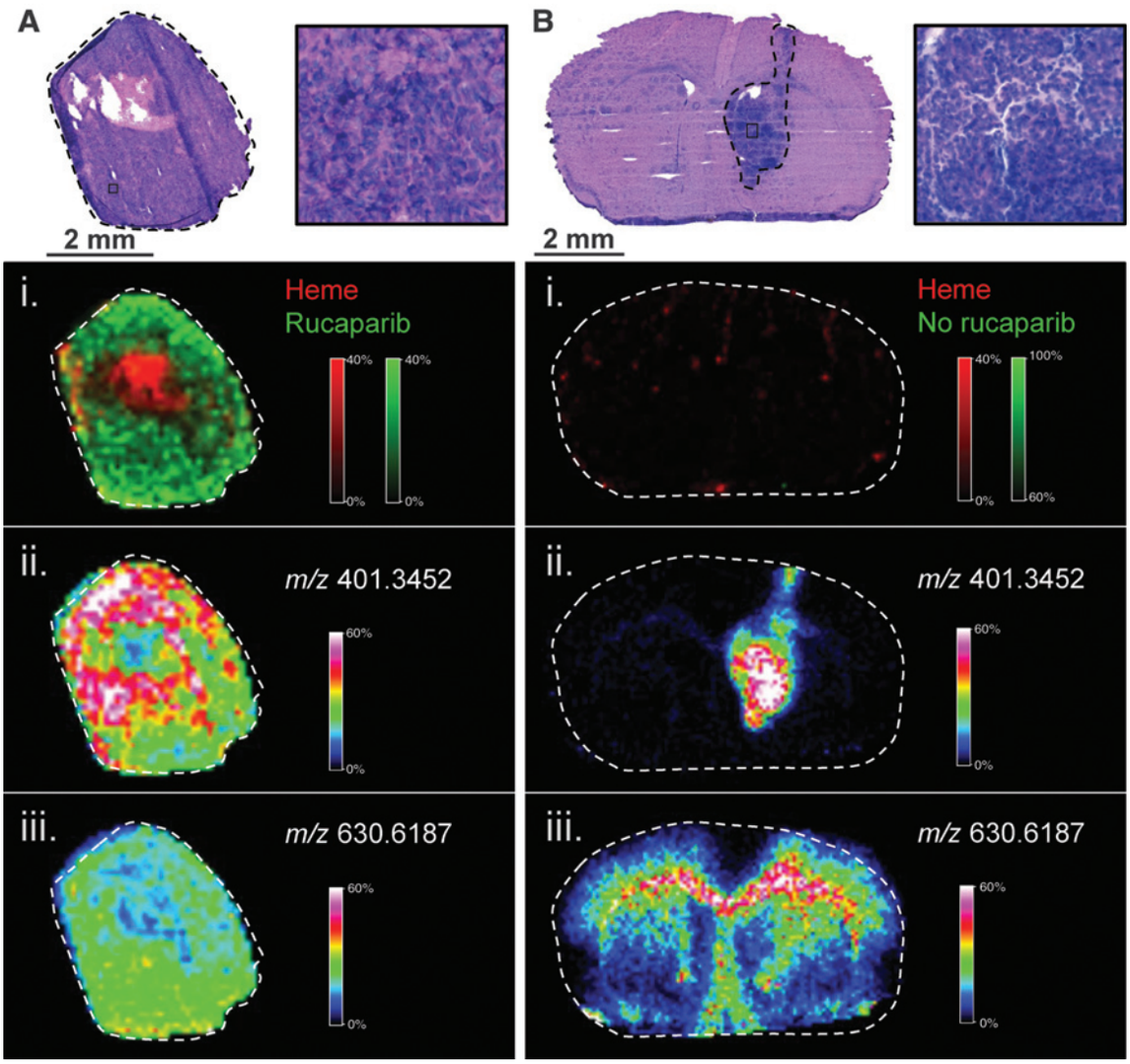

Figure 6.
MALDI-MSI of drug distribution. Mice with established GBM12 flank (A) or orthotopic brain tumors (B) were euthanized thirty minutes after a single dose of rucaparib and processed for MALDI-MSI. Black dotted lines delineate the outline of the tumor tissue in each H/E-stained sister section. White dotted lines delineate the outline of the tissue section from H&E-stained sections. Top, (i) red and green color intensities indicate relative levels of heme, a marker of vasculature, (*m/z* 616.1768 ± 0.001) and rucaparib (*m/z* 324.1507 ± 0.001), respectively. Middle, (ii) shows the distribution of an ion detected in tumor tissue (*m/z* 401.3452 ± 0.001). Bottom, (iii) displays the distribution of an ion detected throughout both brain and flank tumor sections (*m/z* 630.6187 ± 0.001). Results are representative of 3 mice for the orthotopic tumor and 2 mice for the GBM12 flank conditions, respectively.

brain, there was an almost 20-fold increase in the brain-to-plasma ratio in *Mdr1a/b*$^{-/-}$*Bcrp1*$^{-/-}$ knockout mice. A recent study also reported that efflux transport at the BBB restricted brain delivery of rucaparib (40); the current study extends these results by linking limited brain delivery of rucaparib with a lack of treatment efficacy for an otherwise active drug. Numerous other small-molecule inhibitors are excluded from the brain via the efflux activities of MDR1 and BCRP at the BBB (21, 23, 39, 41–45), and similar to the approach taken here, *in vitro* screening for efflux liability may be an effective way to rapidly identify drugs that are more than likely to have limited brain penetration.

The impact of limited drug distribution into normal brain on treatment efficacy for brain tumors has been evaluated in several previous preclinical studies. In a comparison of a PDGF-driven glioma model established in the same FVB mouse models used in this study, significantly higher drug delivery into the brain of the PDGFR inhibitor dasatinib was associated a significant improvement in survival for tumor-bearing *Mdr1a/b*$^{-/-}$*Bcrp1*$^{-/-}$ knockout mice compared with wild-type mice (23). In a murine GL261 model for glioma, the brain impenetrant drug, 5,6-dimethylxanthenone-4-acetic acid (DMXAA), significantly delayed tumor growth of subcutaneous GL261 tumors, but provided no survival extension in intracranial GL261 tumors (46). Similarly, the Wee1 inhibitor MK-1775 combined with temozolomide chemotherapy provided no sensitizing effect in another Mayo GBM xenograft line (GBM22), despite significant sensitizing effects observed in flank models (47). For both the MK-1775 study in GBM22 and the

current study in GBM12, the results suggest that limited accumulation of chemo- or radio-sensitizing drugs within orthotopic brain tumors may have profound impact on limiting the enhancement of a highly active and brain-penetrant therapy such as temozolomide.

The dosage regimen used in this study was derived to mimic the dosing schedule for both rucaparib and temozolomide that is used in the clinic. This dosage regimen was the highest dose of rucaparib (1 mg/kg i.p.) that was tolerated for chronic administration of rucaparib with 50 mg/kg *per os* temozolomide (this provides similar exposure in mice as a dose of 150 mg/m^2 in humans). The maximum rucaparib plasma concentrations following a single 1 mg/kg dose in our preclinical study are about 4 to 5 times lower than the C_{max} in humans reported in the literature (12). Interestingly, even when the rucaparib dose was escalated to 10 mg/kg, rucaparib was still below the limit of detection in the brain by MALDI-MSI. At 1 mg/kg, the exposure of rucaparib in the flank tumor was sufficient to reduce tumor growth, indicating that this dose of rucaparib is not in the subtherapeutic range, but that active efflux at the BBB limits rucaparib brain distribution and efficacy.

Exclusion of drugs from the central nervous system and regions of brain tumors is a significant barrier for development of effective novel therapeutic agents for primary or metastatic brain tumors. At least 7 PARP inhibitors are being assessed in clinical trials but only veliparib (7, 26) and E7016 (48) are known to significantly penetrate the BBB. In a recent study that examined three PARP inhibitors, olaparib was identified as an MDR1 substrate (49). On the basis of the data presented here and the biochemistry of MDR1 within the BBB, these data suggest that olaparib should have limited brain penetration. Consistent with this assumption, a recent phase 0 trial measuring olaparib levels in resected GBM demonstrated a correlation between olaparib concentration and BBB disruption, as measured by dynamic contrast enhancement magnetic resonance imaging (50). Although the conclusion reached by these authors was that olaparib should be suitable for brain tumor therapy, extrapolation of the current data with rucaparib would predict limited efficacy of olaparib or other brain impenetrant PARP inhibitors when combined with temozolomide in GBM.

Disclosure of Potential Conflicts of Interest

D. Calligaris is a consultant/advisory board member for BayesianDx. N.Y.R. Agar is a consultant/advisory board member for Bayesian Dx and inviCRO. N. Curtin has ownership interest (including patents) in Clovis. J.N. Sarkaria reports receiving commercial research grants from Basilea, Sanofi, Genentech, Beigene, Lilly, and Merck. No potential conflicts of interest were disclosed by the other authors.

Authors' Contributions

Conception and design: K.E. Parrish, L. Cen, R.K. Mittapalli, W.F. Elmquist, J.N. Sarkaria

Development of methodology: K.E. Parrish, L. Cen, D. Calligaris, R.K. Mittapalli, A.V. Boddy, N.Y.R. Agar, J.N. Sarkaria

Acquisition of data (provided animals, acquired and managed patients, provided facilities, etc.): K.E. Parrish, L. Cen, J. Murray, D. Calligaris, B.L. Carlson, M.A. Shroeder, J. Sludden, A.V. Boddy, N.Y.R. Agar, N. Curtin, J.N. Sarkaria

Analysis and interpretation of data (e.g., statistical analysis, biostatistics, computational analysis): K.E. Parrish, L. Cen, J. Murray, D. Calligaris, S. Kizilbash, R.K. Mittapalli, B.L. Carlson, J. Sludden, A.V. Boddy, N.Y.R. Agar, N. Curtin, W.F. Elmquist

Writing, review, and/or revision of the manuscript: K.E. Parrish, L. Cen, D. Calligaris, S. Kizilbash, R.K. Mittapalli, A.V. Boddy, N.Y.R. Agar, N. Curtin, W.F. Elmquist, J.N. Sarkaria

Administrative, technical, or material support (i.e., reporting or organizing data, constructing databases): J. Murray, B.L. Carlson, J.N. Sarkaria

Study supervision: B.L. Carlson, N. Curtin, J.N. Sarkaria

Grant Support

This work was supported in part by grants to J.N. Sarkaria from the Mayo Foundation, the NIH (CA141121 and CA127716) and the Brain Tumor Funders Consortium. This work was also supported in part by grants to W.F. Elmquist from the NIH (CA138437) and to both J.N. Sarkaria and W.F. Elmquist from the NIH (NS077921). N.Y.R. Agar was funded by the National Institute of Health Director's New Innovator Award (1DP2OD007383-01), Dana-Farber PLGA Foundation, and Daniel E. Ponton fund for the Neurosciences. K.E. Parrish was supported by the Ronald J. Sawchuk, Edward G. Rippie and American Foundation for Pharmaceutical Education Pre-Doctoral Fellowships.

The costs of publication of this article were defrayed in part by the payment of page charges. This article must therefore be hereby marked *advertisement* in accordance with 18 U.S.C. Section 1734 solely to indicate this fact.

Received July 1, 2015; revised September 11, 2015; accepted September 14, 2015; published OnlineFirst October 5, 2015.

References

1. Stupp R, Mason WP, van den Bent MJ, Weller M, Fisher B, Taphoorn MJ, et al. Radiotherapy plus concomitant and adjuvant temozolomide for glioblastoma. N Engl J Med 2005;352:987–96.
2. Hegi ME, Diserens A-C, Gorlia T, Hamou M-F, de Tribolet N, Weller M, et al. MGMT Gene silencing and benefit from temozolomide in glioblastoma. N Engl J Med 2005;352:997–1003.
3. Bowman KJ, White A, Golding BT, Griffin RJ, Curtin NJ. Potentiation of anti-cancer agent cytotoxicity by the potent poly(ADP-ribose) polymerase inhibitors NU1025 and NU1064. Br J Cancer 1998;78: 1269–77.
4. Tentori L, Leonetti C, Scarsella M, d'Amati G, Portarena I, Zupi G, et al. Combined treatment with temozolomide and poly(ADP-ribose) polymerase inhibitor enhances survival of mice bearing hematologic malignancy at the central nervous system site. Blood 2002;99:2241–4.
5. Miknyoczki SJ, Jones-Bolin S, Pritchard S, Hunter K, Zhao H, Wan W, et al. Chemopotentiation of temozolomide, irinotecan, and cisplatin activity by CEP-6800, a poly(ADP-ribose) polymerase inhibitor. Mol Cancer Ther 2003;2:371–82.
6. Calabrese CR, Almassy R, Barton S, Batey MA, Calvert AH, Canan-Koch S, et al. Anticancer chemosensitization and radiosensitization by the novel poly(ADP-ribose) polymerase-1 inhibitor AG14361. J Natl Cancer Inst 2004;96:56–67.
7. Donawho CK, Luo Y, Penning TD, Bauch JL, Bouska JJ, Bontcheva-Diaz VD, et al. ABT-888, an orally active poly(ADP-ribose) polymerase inhibitor that potentiates DNA-damaging agents in preclinical tumor models. Clin Cancer Res 2007;13:2728–37.
8. Curtin NJ, Szabo C. Therapeutic applications of PARP inhibitors: anticancer therapy and beyond. Mol Aspects Med 2013;34:1217–56.
9. Daniel RA, Rozanska AL, Mulligan EA, Drew Y, Thomas HD, Castelbuono DJ, et al. Central nervous system penetration and enhancement of temozolomide activity in childhood medulloblastoma models by poly(ADP-ribose) polymerase inhibitor AG-014699. Br J Cancer 2010; 103:1588–96.
10. Thomas HD, Calabrese CR, Batey MA, Canan S, Hostomsky Z, Kyle S, et al. Preclinical selection of a novel poly(ADP-ribose) polymerase inhibitor for clinical trial. Mol Cancer Ther 2007;6:945–56.
11. Daniel RA, Rozanska AL, Thomas HD, Mulligan EA, Drew Y, Castelbuono DJ, et al. Inhibition of poly(ADP-ribose) polymerase-1 enhances temozolomide and topotecan activity against childhood neuroblastoma. Clin Cancer Res 2009;15:1241–9.

12. Plummer R, Jones C, Middleton M, Wilson R, Evans J, Olsen A, et al. Phase I study of the poly(ADP-Ribose) polymerase inhibitor, AG014699, in combination with temozolomide in patients with advanced solid tumors. Clin Cancer Res 2008;14:7917–23.
13. Plummer R, Lorigan P, Steven N, Scott L, Middleton MR, Wilson RH, et al. A phase II study of the potent PARP inhibitor, Rucaparib (PF-01367338, AG014699), with temozolomide in patients with metastatic melanoma demonstrating evidence of chemopotentiation. Cancer Chemother Pharmacol 2013;71:1191–9.
14. Bernhard EJ, McKenna WG, Muschel RJ. Cyclin expression and G2-phase delay after irradiation. Radiat Res 1994;138:S64–S7.
15. Ascierto PA, Simeone E, Giannarelli D, Grimaldi AM, Romano A, Mozzillo N. Sequencing of BRAF inhibitors and ipilimumab in patients with metastatic melanoma: a possible algorithm for clinical use. J Transl Med 2012;10:107.
16. Chu EY, Wanat KA, Miller CJ, Amaravadi RK, Fecher LA, Brose MS, et al. Diverse cutaneous side effects associated with BRAF inhibitor therapy: a clinicopathologic study. J Am Acad Dermatol 2012;67:1265–72.
17. Falchook GS, Long GV, Kurzrock R, Kim KB, Arkenau TH, Brown MP, et al. Dabrafenib in patients with melanoma, untreated brain metastases, and other solid tumours: a phase 1 dose-escalation trial. Lancet 2012;379:1893–901.
18. Gibney GT, Sondak VK. Extending the reach of BRAF-targeted cancer therapy. Lancet 2012;379:1858–9.
19. Simeone E, De Maio E, Sandomenico F, Fulciniti F, Lastoria S, Aprea P, et al. Neoplastic leptomeningitis presenting in a melanoma patient treated with dabrafenib (a V600EBRAF inhibitor): a case report. J Med Case Rep 2012; 6:131.
20. Kitange GJ, Mladek AC, Carlson BL, Schroeder MA, Pokorny JL, Cen L, et al. Inhibition of histone deacetylation potentiates the evolution of acquired temozolomide resistance linked to MGMT upregulation in glioblastoma xenografts. Clin Cancer Res 2012;18:4070–9.
21. Agarwal S, Sane R, Gallardo JL, Ohlfest JR, Elmquist WF. Distribution of gefitinib to the brain is limited by P-glycoprotein (ABCB1) and breast cancer resistance protein (ABCG2)-mediated active efflux. J Pharmacol Exp Ther 2010;334:147–55.
22. Carlson BL, Pokorny JL, Schroeder MA, Sarkaria JN. Establishment, maintenance, and in vitro and in vivo applications of primary human glioblastoma multiforme (GBM) xenograft models for translational biology studies and drug discovery. Curr Protoc Pharmacol 2011;52:14.6.1 -.6.23.
23. Agarwal S, Mittapalli RK, Zellmer DM, Gallardo JL, Donelson R, Seiler C, et al. Active efflux of Dasatinib from the brain limits efficacy against murine glioblastoma: broad implications for the clinical use of molecularly targeted agents. Mol Cancer Ther 2012;11:2183–92.
24. Mittapalli RK, Vaidhyanathan S, Sane R, Elmquist WF. Impact of P-glycoprotein (ABCB1) and breast cancer resistance protein (ABCG2) on the brain distribution of a novel BRAF inhibitor: vemurafenib (PLX4032). J Pharmacol Exp Ther 2012;342:33–40.
25. Liu X, Ide JL, Norton I, Marchionni MA, Ebling MC, Wang LY, et al. Molecular imaging of drug transit through the blood-brain barrier with MALDI mass spectrometry imaging. Sci Rep 2013;3:2859.
26. Clarke MJ, Mulligan EA, Grogan PT, Mladek AC, Carlson BL, Schroeder MA, et al. Effective sensitization of temozolomide by ABT-888 is lost with development of temozolomide resistance in glioblastoma xenograft lines. Mol Cancer Ther 2009;8:407–14.
27. Gupta SK, Mladek AC, Carlson BL, Boakye-Agyeman F, Bakken KK, Kizilbash SH, et al. Discordant in vitro and in vivo chemopotentiating effects of the PARP inhibitor veliparib in temozolomide-sensitive versus -resistant glioblastoma multiforme xenografts. Clin Cancer Res 2014;20:3730–41.
28. Gottesman MM, Fojo T, Bates SE. Multidrug resistance in cancer: role of ATP-dependent transporters. Nat Rev Cancer 2002;2:48–58.
29. Austin Doyle L, Ross DD. Multidrug resistance mediated by the breast cancer resistance protein BCRP (ABCG2). Oncogene 2003;22:7340–58.
30. Ambudkar SV, Kimchi-Sarfaty C, Sauna ZE, Gottesman MM. P-glycoprotein: from genomics to mechanism. Oncogene 2003;22:7468–85.
31. Murray J, Thomas H, Berry P, Kyle S, Patterson M, Jones C, et al. Tumour cell retention of rucaparib, sustained PARP inhibition and efficacy of weekly as well as daily schedules. Br J Cancer 2014;110:1977–84.
32. Kalpathy-Cramer J, Gerstner ER, Emblem KE, Andronesi OC, Rosen B. Advanced magnetic resonance imaging of the physical processes in human glioblastoma. Cancer Res 2014;74:4622–37.
33. Pafundi DH, Laack NN, Youland RS, Parney IF, Lowe VJ, Giannini C, et al. Biopsy validation of 18F-DOPA PET and biodistribution in gliomas for neurosurgical planning and radiotherapy target delineation: results of a prospective pilot study. Neuro-oncology 2013;15:1058–67.
34. Earnest FT, Kelly PJ, Scheithauer BW, Kall BA, Cascino TL, Ehman RL, et al. Cerebral astrocytomas: histopathologic correlation of MR and CT contrast enhancement with stereotactic biopsy. Radiology 1988;166:823–7.
35. Blakeley JO, Olson J, Grossman SA, He X, Weingart J, Supko JG. Effect of blood brain barrier permeability in recurrent high grade gliomas on the intratumoral pharmacokinetics of methotrexate: a microdialysis study. J Neurooncol 2009;91:51–8.
36. van Tellingen O, Yetkin-Arik B, de Gooijer MC, Wesseling P, Wurdinger T, de Vries HE. Overcoming the blood-brain tumor barrier for effective glioblastoma treatment. Drug Resist Updat 2015;19:1–12.
37. Lockman PR, Mittapalli RK, Taskar KS, Rudraraju V, Gril B, Bohn KA, et al. Heterogeneous blood-tumor barrier permeability determines drug efficacy in experimental brain metastases of breast cancer. Clin Cancer Res 2010;16:5664–78.
38. Schinkel AH, Jonker JW. Mammalian drug efflux transporters of the ATP binding cassette (ABC) family: an overview. Adv Drug Deliv Rev 2003;55: 3–29.
39. Agarwal S, Manchanda P, Vogelbaum MA, Ohlfest JR, Elmquist WF. Function of the blood-brain barrier and restriction of drug delivery to invasive glioma cells: findings in an orthotopic rat xenograft model of glioma. Drug Metab Dispos 2013;41:33–9.
40. Durmus S, Sparidans RW, van Esch A, Wagenaar E, Beijnen JH, Schinkel AH. Breast cancer resistance protein (BCRP/ABCG2) and P-glycoprotein (P-GP/ABCB1) restrict oral availability and brain accumulation of the PARP inhibitor rucaparib (AG-014699). Pharm Res 2015;32:37–46.
41. Agarwal S, Sane R, Ohlfest JR, Elmquist WF. The role of the breast cancer resistance protein (ABCG2) in the distribution of sorafenib to the brain. J Pharmacol Exp Ther 2011;336:223–33.
42. Mittapalli RK, Vaidhyanathan S, Dudek AZ, Elmquist WF. Mechanisms limiting distribution of the threonine-protein kinase B-RaF(V600E) inhibitor dabrafenib to the brain: implications for the treatment of melanoma brain metastases. J Pharmacol Exp Ther 2013;344:655–64.
43. Oberoi RK, Mittapalli RK, Elmquist WF. Pharmacokinetic assessment of efflux transport in sunitinib distribution to the brain. J Pharmacol Exp Ther 2013;347:755–64.
44. Chuan Tang S, Nguyen LN, Sparidans RW, Wagenaar E, Beijnen JH, Schinkel AH. Increased oral availability and brain accumulation of the ALK inhibitor crizotinib by coadministration of the P-glycoprotein (ABCB1) and breast cancer resistance protein (ABCG2) inhibitor elacridar. Int J Cancer 2014;134:1484–94.
45. Iusuf D, Teunissen SF, Wagenaar E, Rosing H, Beijnen JH, Schinkel AH. P-glycoprotein (ABCB1) transports the primary active tamoxifen metabolites endoxifen and 4-hydroxytamoxifen and restricts their brain penetration. J Pharmacol Exp Ther 2011;337:710–7.
46. Yung R, Seyfoddin V, Guise C, Tijono S, McGregor A, Connor B, et al. Efficacy against subcutaneous or intracranial murine GL261 gliomas in relation to the concentration of the vascular-disrupting agent, 5,6-dimethylxanthenone-4-acetic acid (DMXAA), in the brain and plasma. Cancer Chemother Pharmacol 2014;73:639–49.
47. Pokorny JL, Calligaris D, Gupta SK, Iyekegbe DO, Mueller D, Bakken KK, et al. The efficacy of the Wee1 inhibitor MK-1775 combined with temozolomide is limited by heterogeneous distribution across the blood-brain barrier in glioblastoma. Clin Cancer Res 2015;21:1916–25.
48. Russo AL, Kwon HC, Burgan WE, Carter D, Beam K, Weizheng X, et al. In vitro and in vivo radiosensitization of glioblastoma cells by the poly (ADP-ribose) polymerase inhibitor E7016. Clin Cancer Res 2009;15: 607–12.
49. Lawlor D, Martin P, Busschots S, Thery J, O'Leary JJ, Hennessy BT, et al. PARP inhibitors as p-glyoprotein substrates. J Pharm Sci 2014;103: 1913–20.
50. Chalmers A, Jackson A, Swaisland H, Stewart W, Halford S, Molife R, et al. Olaparib penetrates glioblastoma at therapeutic levels: results of stage 1 of the OPARATIC trial; a phase I study of olaparib in combination with temozolomide in patients with relapsed glioblastoma.J Clin Oncol 32:5s (suppl; abstr 2025).